Int. J. Heat Mass Transfer. Vol. 36, No. 12, pp. 3043–3057, 1993
Printed in Great Britain

0017–9310/93 $6.00 + 0.00

Augmentative heat transfer in a vertical 2-pass tube through an air box by use of strip type inserts

SHOU-SHING HSIEH† and MAO-YU WEN
Department of Mechanical Engineering, National Sun Yat-Sen University, Kaohsiung, Taiwan 80424, R.O.C.

(*Received* 29 *June* 1992 *and in final form* 15 *December* 1992)

Abstract—This work presents and discusses an experimental information of the augmentation of heat transfer in a vertical 2-pass tube through an air box by use of different inserts (strip type inserts-longitudinal strip (LS), crossed-strip (CS) and regularly interrupted strip (RIS)) in a crossflow heat exchanger. Flow visualization as well as the interferogram of the temperature field inside/outside the tube were made and analyzed. Correlations for Nusselt number and pressure drop factor are reported and comparisons of these results with those of smooth tubes are also discussed. In addition, the performance has been evaluated by two different criteria based on both constant pumping power and constant heat duty, which suggest the use of these inserts in certain ranges of the Reynolds numbers in the present crossflow heat exchanger.

1. INTRODUCTION

AUGMENTATION of heat transfer and improvement of the power efficiency of devices in which processes occur are the principal goals in the development of convective heat exchangers. Among the many techniques (both passive and active) investigated for augmentation of heat transfer rates inside circular tubes, a wide range of inserts has been utilized, particularly when turbulent flow is considered: tapered spiral inserts, packing, rings, discs, streamlined shapes, mesh inserts, and spiral brush inserts (Bergles [1]). The mesh or spiral brush inserts were used by Megerlin *et al.* [2] to enhance turbulent heat transfer in short channels subjected to a high heat flux. Uttarwar and Raja Rao [3] reported on isothermal performance to servotherm medium grade oil in laminar flow in one smooth tube and seven wire coil-inserted tubes of varying wire diameter and pitch of wire coil. The results indicated that as much as a four-fold improvement can be obtained in laminar flow heat transfer coefficient using these tubes. In general, it is found that these inserts are frequently used in very few practical turbulent situations for the reasons of plugging or fouling, and structure consideration. For generality and simplicity, the present study will only focus on a single tube with turnaround (air box) instead of a tube bundle type crossflow heat exchanger.

The secondary flows caused by centrifugal force in curved pipes and by buoyancy force in a crossflow heat exchanger by means of strip inserts are known to be important in forced convection heat transfer and the related literature is quite extensive due to their practical importance in heat transfer equipment applications [4, 5]. The geometry of the 180°-bend was conducted by Azzola and Humphrey [6]. They analyzed the convection caused by the secondary flow and modifications to the fluctuating velocity in order to determine the level of heat transfer coefficient. In addition, the local heat transfer measurements in and downstream from a U-bend were reported by Moshfeghiah and Bell [7]. Furthermore, recently, flow visualization studies of secondary flow patterns and centrifugal instabilities in curved circular and semicircular pipes were reported [8]. Flow visualization studies on secondary flow patterns in straight tubes downstream of a 180°-bend and in isothermally heated horizontal tube were conducted by Cheng and Yuen [9, 10].

The present study is aimed at providing detailed information about the forced convective heat transfer coefficient and thermal field in straight tube upstream/downstream of a 180°-bend in an air box under developing flow condition. In addition, it will examine whether the pressure drop associated with the strip type inserts can be reduced without seriously impairing the heat transfer augmentation. Furthermore, flow visualization studies on secondary flow patterns inside the air box and at its exit have been complemented. In order to gather the qualitative information of the temperature for the test tube, the interferogram technique was finally applied to the present study. The experimental setup has been designed for a geometry of the 180°-bend in an air box. Strip inserts with three different configurations are considered as the enhancement devices within the crossflow heat exchanger tubes. Figure 1(a) shows the schematic of the present study. Inserts including longitudinal strip (LS), crossed-strip (CS), and regularly interrupted strip (RIS) type are shown in Fig.

† Author to whom correspondence should be addressed.

NOMENCLATURE

A	area occupied by the fluid for the tube section [m^2]
C_P	isobaric specific heat [$kJ\,kg^{-1}\,K^{-1}$]
D	tube inner diameter [m]
E_1	$[\varepsilon([22]) - \varepsilon(\text{present})/\varepsilon(\text{present})]$ (%)
E_2	$1-[(mC_p)_c(T_{co}-T_{ci})/(mC_p)_h(T_{hi}-T_{ho})]$ (%)
Eu	dimensionless pressure drop factor
f	friction factor, $(\Delta P/\frac{1}{2}\rho v^2)(D/L) = Eu(D/L)$
g	acceleration due to gravity [$m\,s^{-2}$]
h	convective heat transfer coefficient [$W\,m^{-2}\,K^{-1}$]
k	thermal conductivity [$W\,m^{-1}\,K^{-1}$]
L	length of the test tube [m]
Ntu	number of transfer unit UA_o/c_{min}
Nu	Nusselt number, hD/k
Δp	pressure drop [$kg\,s^{-2}\,m^{-1}$]
Pr	Prandtl number, v/α
Q	heat flux [$J\,s^{-1}$]
R_1	effectiveness evaluation criterion, constant pumping power
R_2	effectiveness evaluation criterion, constant heat duty
Re	Reynolds number, vD/v
T_{bi}	inlet bulk mean temperature of the fluid [°C]
T_{bo}	outlet bulk mean temperature of the fluid [°C]
T_f	reference fluid temperature, $0.5(T_{wz}+T_{bz})$ [°C]
T_{wz}	average circumference-wall temperature at any z [°C]
v	inlet velocity of cold air in tube side channel [$m\,s^{-1}$]
z	streamwise direction coordinate [m].

Greek symbols

δ	strip thickness [m]
Δ	thickness of space emptied by the RIS insert
ε	exchanger heat transfer effectiveness, $\dot{Q}_{act}/\dot{Q}_{max}$
v	kinematic viscosity [$m^{-2}\,s^{-1}$]
ρ	density [$kg\,m^{-3}$].

Subscript

act	actual situation
BR	tube without inserts
c	cold air in the tube side
CS	crossed-strip type inserts
fl	full-length inserts
h	hot air in the shell side
i	inlet
insert	with insert
LS	longitudinal strip type inserts
max	maximum
min	minimum
no	without insert
o	outlet
RIS	regularly interrupted strip type inserts.

1(b). Flow uniformity for both velocity and temperature measurements at inlet and outlet of test section has been examined.

Experiments carried out with air as the working fluid are presented and discussed. They (not for thermal/flow visualization) were conducted over the following ranges of independent parameters:

hot air temperature	$T_{hi} = 90, 110$°C
shell side Reynolds number	$Re_h = 4300$
tube side Reynolds number	$8989 \leqslant Re_c \leqslant 135\,635$
strip type inserts	LS, CS, RIS.

2. EXPERIMENTAL APPARATUS AND PROCEDURE

The experiments were performed in a closed loop experimental facility as shown in Fig. 1. The loop consisted of two blowers (7.5 and 3 HP), a 22.5 kW electrical heater, the test section (Fig. 2) and a regulation valve. Strip type inserts were made from 1.5 mm thick carbon steel strip, the width of which was 1 mm less than the inside diameter of the test section tube. The crossed-strip type inserts made out of spot welded longitudinal strip inserts are shown in Fig. 1(b). The regularly interrupted strip type inserts were made from interruptedly cut longitudinal strip inserts. All inserts were spot-welded to the ends with steel rods for fixing in the test section tubes. The length of the entire closed loop for shell side wind tunnel was about 18 m and for the tube side tunnel was about 11 m. The electrical heating device consisted of 15 finned type electrical heating rods with a total power output of 22.5 kW. The inlet temperature of hot air was controlled by an ON–OFF and a proportional integral-differential (PID) systems, in which 13.5 kW was controlled by an ON–OFF system and the other 9 kW was controlled by a PID system. The variation of the inlet temperature of hot air was $\pm 0.2\%$ about the temperature setting. The outer surface of the entire apparatus was insulated by fiberglass insulating material. The conduction and radiation losses, after careful calculations, were 2.5 and 2.2% of the net convective heat transfer rate, respectively.

The test section used in the present study was a rectangular 80 cm high and 40 cm wide wind tunnel. The test section consists of the shell side and tube side.

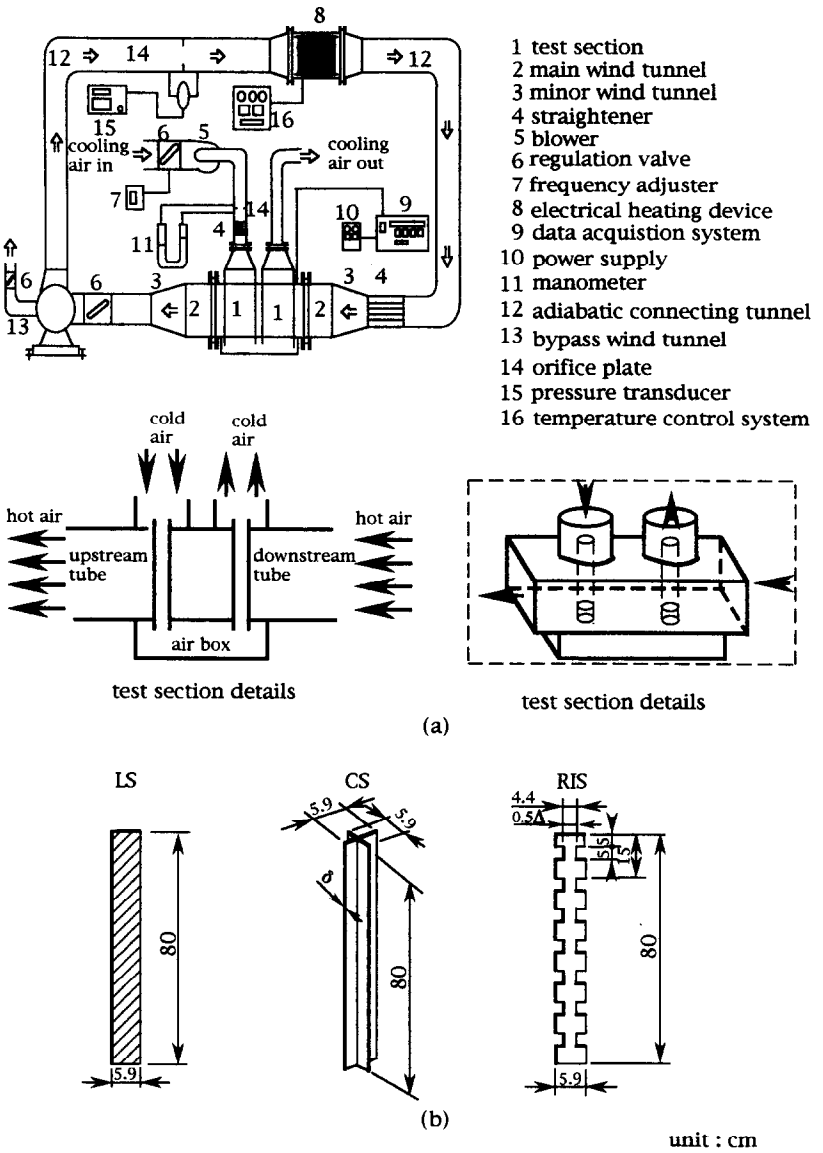

FIG. 1. (a) Schematic view of experimental apparatus, (b) geometry of strip type inserts.

Hot air flowing through the shell side and cold air through the tube side were driven, respectively, by 7.5 and 3 HP frequency adjusted high speed centrifugal blowers. The tube was 72 mm in diameter and 6 mm in thickness, and it was made out of carbon steel. The total volumetric flow rate of shell side and tube side were measured by an orifice meter ($\beta = 0.7$) which was attached to a manometer and/or a pressure transducer. In addition, for the velocity measurement in the inlet/outlet of the test tube, two pressure ports in the pitot tube are connected to DP-103 transducers, the measured pressure by means of a CD-18 digital manometer system is converted into voltage automatically and finally converted into reading in the velocity at the different thermocouple positions (shown in the section $A'-A'$ of Fig. 2). The hot wire was also used in the same position to examine the flow uniformity for the cold air at the inlet/outlet. The inlet and outlet temperatures of hot and cold air were measured by the AWG-24 K-type thermocouples which were uniformly placed at the inlet and outlet cross section of the shell side and tube side wind tunnel, respectively. The thermocouple arrangements are shown in Fig. 2. The thermocouple output was fed to the data acquisition system coupled with an IBM personal computer for data reduction and analysis.

To examine the flow structure, flow visualization experiments were conducted for the surrounding field of the single tube and air box in the tube side. The smoke generation method was applied with a CCl_4+TiCl_4 mixture (mixing ratio 1:10) and air as

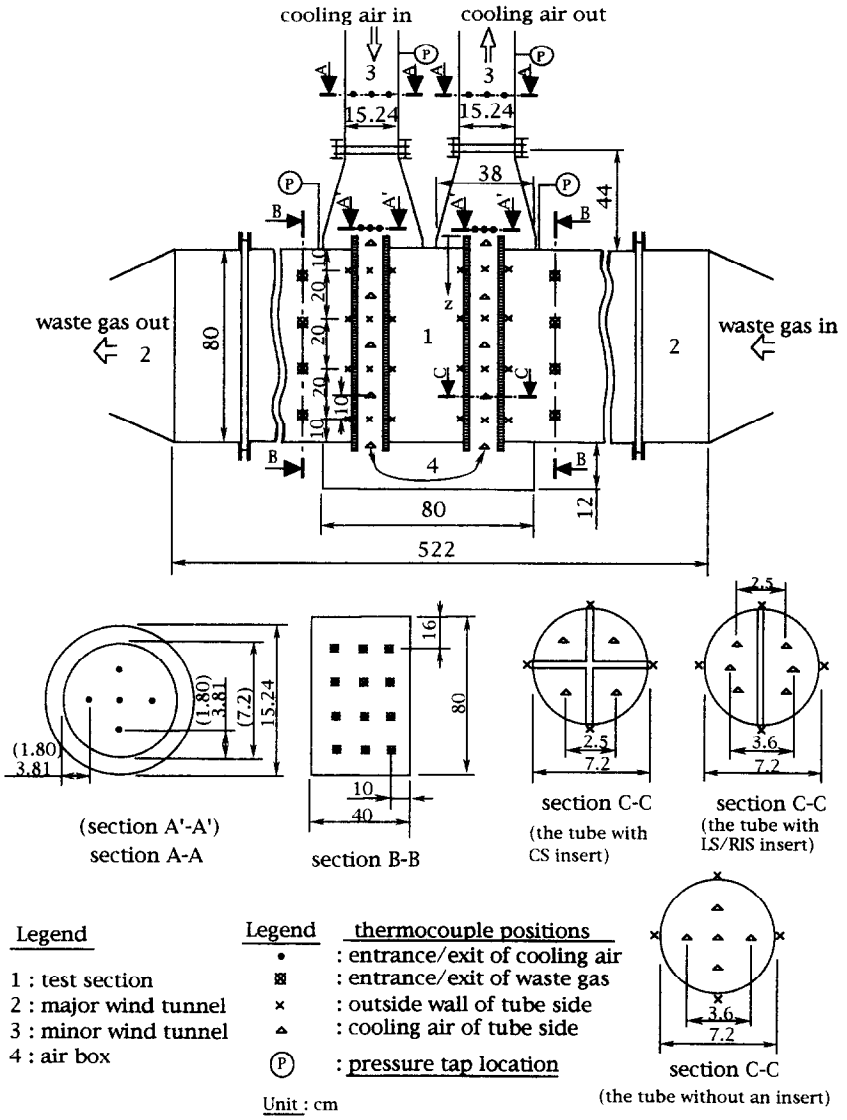

FIG. 2. Detailed position for quantitative temperature and pressure measurements.

the convection medium to visualize the flow. The illumination of the smoke was done by using a slide projector as a light source shining through a narrow slit so as to produce a plane of light. All photographs were taken with a Canon T70 camera on FUJICOLOR ISO 1600 film with exposure times of 1/8–1/15 s.

In addition, for further understanding of the thermal characteristics of the study, the laser holographic interferometry was used in this study. It is essentially similar to that described by Aung and O'Regan [11] and shown schematically in Fig. 3. Coherent light (632.8 μm) from a 35 mW Spectra-Physics mode 124-B He–Ne laser is split into an object beam and a reference beam is expanded to a 90 mm planar wave via a $\times 20$ microscopic objective, a $\times 60$ microscopic objective, and two collimating lenses (diameter 12.7 cm). Pinholes of 20 μm diameter are located at the focal points of the microscopic objectives in order to eliminate intensity variations in the wave fronts. The two wave fronts intersect at the photographic plate (here at an angle of 30°) and produce a hologram when the photographic emulsion is exposed simultaneously to the two beams and then developed in situ. The interferometer components and test section are mounted securely to a 1.4×2.0 m vibration-free optical table.

3. UNCERTAINTY ANALYSIS

A Solartron ORION A automatic data acquisition system was used for data collection. The thermocouple outputs were measured with ± 1 μV resolution which results in ± 0.01°C sensitivity. A conservative estimate of the accuracy of the temperature measurement is ± 0.1°C. The voltage input to each

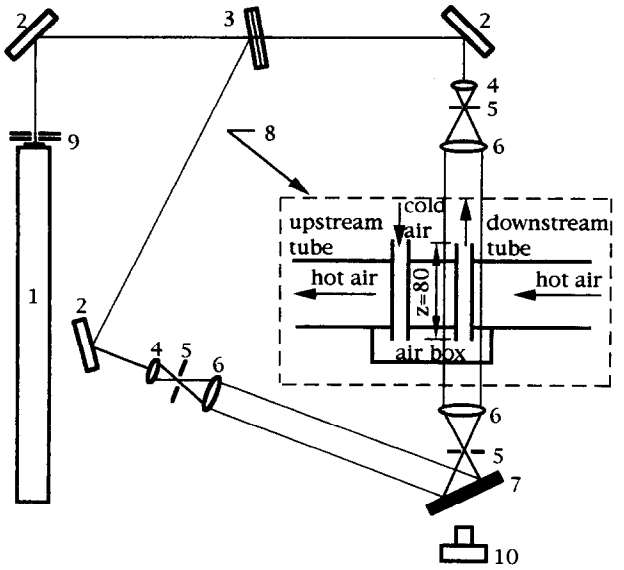

FIG. 3. Schematic of holographic interferometer for thermal field: 1. helium–neon laser; 2. mirror; 3. beam splitter; 4. objective lens; 5. pinhole; 6. collimating lens; 7. holographic plate; 8. test section; 9. shutter; 10. camera.

finned type heater was measured with a sensitivity of ± 1 mV and an accuracy of $\pm 0.1\%$. The total power output of electrical heating device was 22.5 kW, and a proportional integral differential (PID) control system was used. Several runs were conducted in which the voltage and the current for the circuit were measured, and the calculated power output was highly stable. This procedure results in a maximum uncertainty of $\pm 2.5\%$ for the calculated power output. The thermophysical properties of the air were assigned an uncertainty of $\pm 2.5\%$. This was based on the observed variations in the reported values in the literature.

The estimated uncertainties in the Re_h, Re_c, f, and Nu_m are 2.8–4.5, 4.19–4.20, 4.01–8.16, and 2.18–7.25%, respectively. The energy losses by conduction and radiation are 4% of the total energy output of the electrical heating device, respectively. It should be noted that the uncertainties in these parameters were calculated by least square deviation method.

4. RESULTS AND DISCUSSION

An extensive study was made of the heat transfer augmentation effect in a crossflow heat exchanger by means of strip type inserts for the downstream/upstream straight tube of a bend in an air box. There were 44 different cases (see Table 1) to be tested to gather extensive data for analyzing experimental information of the heat transfer enhancement. In addition, eight flow field visualizations and four interferograms showing isotherms will be presented and discussed in this study. Furthermore, a comparison between results and a standard correlation [12] for the smooth tube without an insert will also be made. Examination of flow uniformity for the cold air at inlet/outlet by using the pitot tube and hot wire found that the flow uniformity of the cold air at inlet/outlet was acceptable. The performance of the apparatus and the measuring technique were deemed satisfactory.

4.1. *Flow visualization*

The main interest here is to study the complicated flow patterns resulting from the interaction among centrifugal force, buoyancy force, and the geometry in an air box. The present results focus on the local steady-state behavior. Flow visualization was made by means of a smoke generator under the steady-state condition. The steady-state condition was determined when the variation of temperature of the tube wall was less than 1% of that of its previous value. It usually took 1 h to reach a steady state. The schematic representations with proper view of the flow structure for the present study were shown in the proper position for each photograph made by flow visualization.

Results of flow visualization near the exit of the downstream tube with the inserts for the Reynolds number $Re_c = 3000$ were shown in Figs. 4(a)–(e). Figures 4(a)–(d) stand for the top view of smoke patterns for strip inserts—longitudinal strip (LS), crossed-strip (CS), and regularly interrupted strip (RIS). For the regularly interrupted strip, flow visualizations at two different positions were made. Furthermore, in order to bring a better understanding for the RIS insert, the side view of smoke pattern for RIS at the streamwise direction is also shown in Fig. 4(e). In general, based on the top view, these flow patterns have the symmetric vortex cells. Also, as the Reynolds number increases, it was found that the strength of the symmetric vortices was enhanced (not shown here). Fig-

Table 1. Measured/calculated values of the relevant parameters

Bare tube

Re_h	$\dot{m}_h$ [kg s^{-1}]	T_{hi} [°C]	$\dot{m}_c$ [kg s^{-1}]	Re_c	C_{min}/C_{max}	Ntu	ε (present)	ε (Ref. [22])	E_1 (%)	E_2 (%)
4300	0.524	110	0.021	24 598	0.0148	0.279	0.4022	0.3226	−19.8	5.2
4300	0.524	110	0.043	49 426	0.0277	0.248	0.3373	0.2826	−16.2	3.7
4300	0.524	110	0.061	69 771	0.0405	0.223	0.2788	0.2512	−9.9	7.1
4300	0.524	110	0.081	93 450	0.0605	0.192	0.2504	0.2131	−14.9	7.7
4300	0.524	110	0.101	116 094	0.0815	0.167	0.2011	0.1832	−8.9	9.5
4300	0.524	110	0.118	135 635	0.1150	0.139	0.1638	0.1505	−8.1	3.1
4300	0.524	90	0.008	8989	0.1271	0.131	0.1668	0.1413	−15.3	5.3
4300	0.524	90	0.015	16 782	0.1541	0.116	0.1344	0.1242	−7.6	1.6
4300	0.524	90	0.032	36 667	0.1920	0.099	0.1141	0.1060	−7.1	2.9
4300	0.524	90	0.067	77 013	0.2202	0.085	0.1080	0.0955	−11.6	4.8
4300	0.524	90	0.116	133 335	0.2241	0.082	0.1003	0.0943	−6.0	5.1

LS-insert

Re_h	$\dot{m}_h$ [kg s^{-1}]	T_{hi} [°C]	$\dot{m}_c$ [kg s^{-1}]	Re_c	C_{min}/C_{max}	Ntu	ε (present)	ε (Ref. [22])	E_1 (%)	E_2 (%)
4300	0.524	110	0.021	24 598	0.0148	0.320	0.4563	0.3783	−17.1	3.7
4300	0.524	110	0.043	49 426	0.0277	0.331	0.4190	0.3947	−5.8	9.4
4300	0.524	110	0.061	69 771	0.0405	0.311	0.3189	0.3677	15.3	8.3
4300	0.524	110	0.081	93 450	0.0605	0.270	0.3175	0.3131	−1.4	4.2
4300	0.524	110	0.101	116 094	0.0815	0.232	0.2537	0.2641	4.1	3.5
4300	0.524	110	0.118	135 635	0.1150	0.185	0.1991	0.2057	3.3	6.6
4300	0.524	90	0.008	8989	0.1271	0.172	0.2004	0.1900	−5.2	8.2
4300	0.524	90	0.015	16 782	0.1541	0.149	0.1639	0.1628	−0.7	3.3
4300	0.524	90	0.032	36 667	0.1920	0.124	0.1398	0.1338	−4.3	6.4
4300	0.524	90	0.067	77 013	0.2202	0.111	0.1254	0.1190	−5.1	4.7
4300	0.524	90	0.116	133 335	0.2241	0.109	0.1230	0.1167	−5.1	2.4

CS-insert

Re_h	$\dot{m}_h$ [kg s^{-1}]	T_{hi} [°C]	$\dot{m}_c$ [kg s^{-1}]	Re_c	C_{min}/C_{max}	Ntu	ε (present)	ε (Ref. [22])	E_1 (%)	E_2 (%)
4300	0.524	110	0.021	24 598	0.0148	0.346	0.4641	0.4207	−9.4	4.5
4300	0.524	110	0.043	49 426	0.0277	0.315	0.4201	0.3723	−11.4	6.3
4300	0.524	110	0.061	69 771	0.0405	0.305	0.3580	0.3594	0.4	8.9
4300	0.524	110	0.081	93 450	0.0605	0.229	0.2839	0.2595	−8.6	6.3
4300	0.524	110	0.101	116 094	0.0815	0.184	0.2295	0.2038	−11.2	7.7
4300	0.524	110	0.118	135 635	0.1150	0.141	0.1740	0.1528	−12.2	2.4
4300	0.524	90	0.008	8989	0.1271	0.131	0.1744	0.1413	−19.0	3.9
4300	0.524	90	0.015	16 782	0.1541	0.112	0.1419	0.1196	−15.7	7.9
4300	0.524	90	0.032	36 667	0.1920	0.098	0.1183	0.0997	−15.7	10.2
4300	0.524	90	0.067	77 013	0.2202	0.089	0.1018	0.0866	−17.7	7.5
4300	0.524	90	0.116	133 335	0.2241	0.084	0.1017	0.0873	−14.2	4.4

RIS-insert

Re_h	$\dot{m}_h$ [kg s^{-1}]	T_{hi} [°C]	$\dot{m}_c$ [kg s^{-1}]	Re_c	C_{min}/C_{max}	Ntu	ε (present)	ε (Ref. [22])	E_1 (%)	E_2 (%)
4300	0.524	110	0.021	24 598	0.0148	0.451	0.5659	0.5710	0.9	9.8
4300	0.524	110	0.043	49 426	0.0277	0.350	0.4338	0.4217	−2.8	5.2
4300	0.524	110	0.061	69 771	0.0405	0.335	0.3623	0.4014	10.8	8.9
4300	0.524	110	0.081	93 450	0.0605	0.249	0.2975	0.2853	−4.1	7.3
4300	0.524	110	0.101	116 094	0.0815	0.198	0.2321	0.2210	−4.8	7.4
4300	0.524	110	0.118	135 635	0.1150	0.150	0.1762	0.1634	−7.3	6.7
4300	0.524	90	0.008	8989	0.1271	0.139	0.1776	0.1506	−15.2	9.5
4300	0.524	90	0.015	16 782	0.1541	0.118	0.1450	0.1265	−12.7	5.7
4300	0.524	90	0.032	36 667	0.1920	0.099	0.1192	0.1049	−9.7	5.8
4300	0.524	90	0.067	77 013	0.2202	0.088	0.1039	0.0928	−10.7	4.1
4300	0.524	90	0.116	133 335	0.2241	0.087	0.1027	0.0915	−10.9	4.3

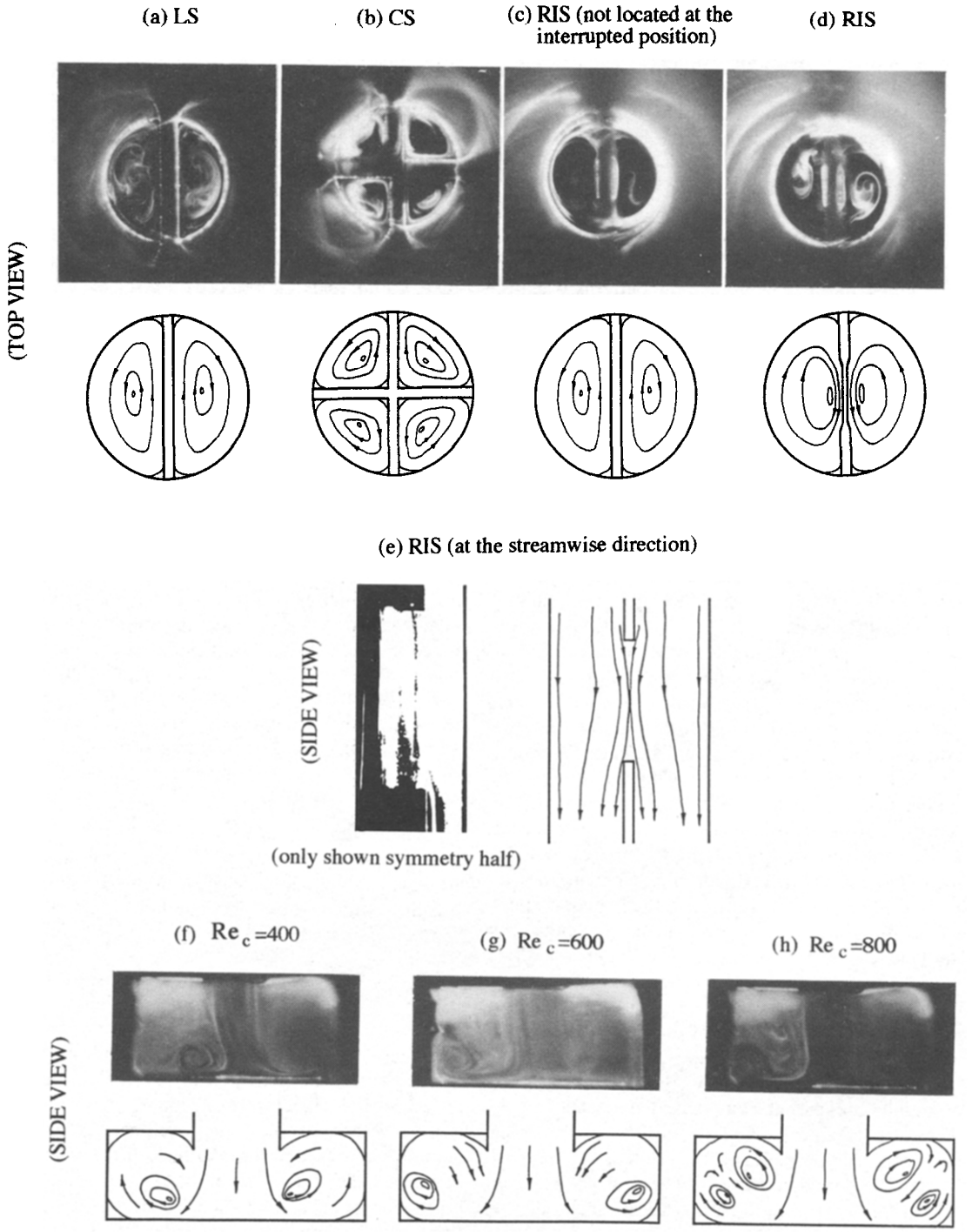

FIG. 4. Smoke patterns and schematic representations near exit of downstream tube with different type inserts (a)–(e) at $Re_c = 600$ and in air box for various Reynolds numbers (f)–(h).

ure 4(a) basically shows a pair of symmetric vortices within the space for a tube with LS insert. Similarly, two pairs of symmetric vortex cells inside the cross section for the CS insert are shown in Fig. 4(b). This is perhaps because the secondary flow was formed and was due to the complex interaction among centrifugal, buoyancy forces, and the special geometry of the air box when the air flowing through the air box. The complicated secondary flow phenomenon persisted until the flow reached the exit of the downstream tube. In addition, Figs. 4(c) and (d) also possess a pair of vortex cells. However, the intensity of the vortex shown in Fig. 4(d) is much larger than the one shown in Fig. 4(c) due to the presence of the interrupted strip. This also indicates that the RIS insert seems to have a stronger turbulence. Figure 4(e)

shows smoke pattern within two consecutive RIS. This photograph only shows the right hand side of the central axis due to the symmetry of the flow pattern and the limit of light source of the slide projector. The flow separated at the trailing edge of RIS (not interrupted portion) and reattached at the leading edge of the next RIS due to a sudden change of the geometry. Meanwhile, the main flow moves to the center with a higher velocity which results in nearly stagnant flow existing in the top and bottom of the concavity.

Figures 4(f)–(h) show the flow patterns when the cold air flowing into the air box for the Reynolds numbers $Re_c = 400$, 600, and 800. It can be seen that the air flow produces two recirculation regions due to the mutual influences of air flow and air collision with the bottom plate of the air box at $Re_c = 400$ shown in Fig. 4(f). Basically, the formation of these two vortex regions is due to the fluid flowing toward the right side and, then, colliding with the vertical wall of the air box. Thereafter, it is inflecting to the top plate of the air box. Meanwhile, the cold air near the upper plate in the air box is frequently processing heat transfer with hot air in the shell side at the top plate. Because of the squeeze effect caused by the expansion of cold air near the top plate in the air box, the fluid flow inflected to the hot region near the top plate of the air box is turned downward. Consequently, the circulation is formed at the lower region near the bottom plate. Figure 4(g) shows that, when Re_c equals 600, the flow patterns of cold air within the air box are similar to those at $Re_c = 400$. However, the rotating centers of these two vortices are moved a little bit toward the vertical wall of the air box due to the higher Re_c. As the Reynolds number continues to increase, the rotating center of these two vortices moves slightly upward, and its intensity is enhanced until the cells may not have enough energy to maintain its recirculating motion. This is because the velocities of the main flow in the vortex region near the lower corner are so fast that the slow motion in the vortex region near the upper plate was unable to keep its original path. Simultaneously, these two cells were eventually broken into four cells at $Re_c = 800$ as evidenced by Fig. 4(h). The large vortices at the lower corner forced the small vortices near the top plate to rotate. This would promote the heat transfer between cold air in the air box and hot air in the shell side.

4.2. *Qualitative description of the temperature field*

The interferograms of the temperature field inside/outside the tube in the infinite fringe mode at the central section of the downstream tube with $Re_h = 1000$, $T_{h,i} = 45°C$, $Re_c = 500$ are presented in Fig. 5(a) for bare tube and Figs. 5(b)–(d) for three different inserts. In general, it is found that the configuration of the resulting fringes for these four photographs is nearly the same. It indicates that the temperature field around the outside of the test tube was not clearly influenced by the different inserts at the same Re_h and Re_c. As usual, when fringes become thinner and get closer to each other, this implies a region of high heat transfer which can be seen from Figs. 5(a)–(d). The fringes outside the test tube are closely packed for the test tube faced at the hot fluid flow, and to be sparsely packed for the back of the test tube. It indicates that the higher heat transfer occurred upstream while the lower one is downstream. Taking further inspection of Figs. 5(c) and (d), it is clearly observed that the higher order fringes possess high curvature in a region outside the tube. It implies that the concave arc-shaped isotherms in this region are directly related to the flow separation/recirculation. It is long recognized that when the flow separated/recirculated the isotherms would appear flat (for instance, Chang *et al.* [13]). In addition, in Fig. 5(a) the interferograms for the fluid inside the BR show an approximate 'M-type' distribution. Its minimum temperature locates at the center of the lower half of the tube. The temperature gradient near the internal wall seems high especially near the lower wall. The thermal stratification occurred at the upper core region. These characteristics are similar to the interferogram made by Yousef and Tarsasuk [14] investigating the combined free/forced convection in a horizontal isothermal tube. Incidentally, Figs. 5(b)–(d) show the interferograms with three different inserts. It is found that the temperature profiles are symmetric and coincide with the previous results based on flow visualization shown in Figs. 4(a)–(c).

4.3. *Heat transfer results*

The tube side overall heat transfer results were evaluated by averaging the heat transfer for the downstream/upstream tube. The length-averaged Nusselt number was defined as

$$\overline{Nu} = \frac{\bar{h}D}{k} = \left(\frac{Q}{\pi Dl}\right)\left(\frac{1}{L}\int_0^L \frac{\mathrm{d}z}{T_{wz} - T_{bz}}\right)\left(\frac{D}{k}\right) \quad (1)$$

where $Q = \dot{m}c_p(T_{bo} - T_{bi})$. The local values of the thermophysical properties of air were obtained at a reference fluid temperature of $T_f = 0.5(T_{wz} + T_{bz})$. T_{wz} is an average of four circumferenced wall temperatures at a fixed position of the z direction (shown in Fig. 2). The bulk temperature T_{bz} at a certain z position is roughly evaluated by an average of the local fluid temperatures for the section of the thermocouple position (the thermocouple arrangements for the tube with/without an insert were shown in the section C-C of Fig. 2).

A dimensionless representation of Nusselt number is presented in Fig. 6(a). It is shown that the tube with insert usually has a better heat transfer rate than the one without insert in the upstream/downstream tube. Based on the downward flow in the upstream tube, for higher Reynolds numbers ($Re_c > 2 \times 10^5$) it strongly displays that LS insert has the best heat transfer performance, followed by CS and RIS, respectively.

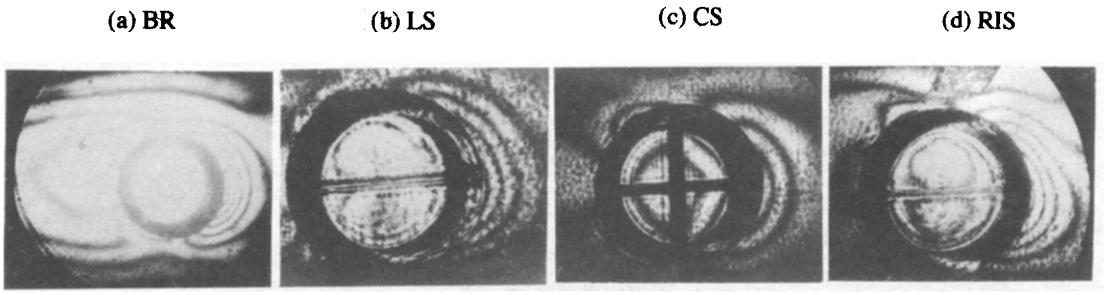

FIG. 5. Interferograms at $z = 40$ cm, $Re_h = 1000$, $T_{h,i} = 45°C$, and $Re_c = 500$ for various insert conditions (a)–(d).

While for lower Reynolds numbers ($Re_c \leqslant 2 \times 10^5$), it shows that CS insert has the highest heat transfer performance, the others are RIS and LS, respectively. In addition, for the upward flow in the downstream tube with higher Reynolds numbers ($Re_c > 2 \times 10^5$), it is found that the tube with LS insert among those three different inserts has the best heat transfer rate, the others are CS and RIS inserts, respectively. Whereas, for the lower Reynolds numbers ($Re_c < 3 \times 10^4$) the tubes with RIS inserts have the best heat transfer rate, followed by CS and LS. Taking a closer examination, when the Reynolds number increases, it can be found that the tube with fixed insert enhances the heat transfer for the tube with LS insert is higher than that of the tube with the other inserts (CS and RIS).

It is common sense that when the forced and free convection flows are passed by a heated surface in the upward direction for a laminar flow the heat transfer is enhanced, whereas when they are in opposition the heat transfer is reduced. This is because the buoyancy effect augments/reduces the heat transfer. However, the situation is quite different for turbulent flow under study. With the forced and free convection flows in the same direction, the local heat transfer coefficient is significantly lower than those for forced flow alone. This is because localized laminarization of the flow due to buoyancy had proved to be the major reason of the sharp peak in the wall temperature (present results coincide with those, but not shown here) which have been reported in a number of papers (see, for instance, Carr *et al.* [15] and Abdelmeguid and Spalding [16]). Furthermore, according to the results of Nackson and Hall [17], the value of buoyancy parameter $1000\ Gr/Re^{2.7}Pr^{0.5}$ for the present study is less than one. Consequently, the heat transfer is certainly enhanced in the downward/upward flow. This coincides with the results reported by Nackson and Hall [17]. Moreover, Baughn *et al.* [18] and Ohad and Sparrow [19] reported that localized laminarization is discovered in a tube situated downstream of a bend for turbulent flow. The fluid flows through an air box, and then turns back into the entrance of downstream tube. This is quite similar to a 180°-bend. Consequently, the buoyancy and centrifugal force would remarkably influence the thermal and flow field. In order to examine the reliability of the present study, a correlation showing the tube without any insert for the previous results [20] was displayed in Fig. 6(a). It can be shown that the heat transfer rate between the present study and previous result [20] for the downflow in the bare tube is almost the same. The maximum difference is within 4.1%. The experimental result for the present study should be much higher than the one in ref. [20] for the upflow. This is because the fluid flowing through the air box results in the secondary flow, which enhances the heat transfer. Taking a further examination, the tube side overall heat transfer with various Reynolds numbers was made and shown in Fig. 6(b). It strongly implies that for lower Reynolds number ($Re_c < 3 \times 10^4$) the tube with RIS insert has the best heat transfer, followed by CS, LS, and BR, respectively. In contrast, for the higher Reynolds numbers ($Re_c > 1.1 \times 10^5$) the tube with LS has the highest heat transfer, followed by CS, RIS, and BR, respectively. In addition, Fig. 6(b) also indicates that the result of the overall mean Nusselt number (including the upstream/downstream tube) for the bare tube of the present study is slightly higher than the values of the Dittus–Boelter equation [21]. It can be clearly seen from the previous results and discussion for the upstream/downstream tubes that the air box results in the heat transfer rate being enhanced. Finally, in order to develop an acceptable empirical solution for industrial design applications, eight sets of correlations for average Nusselt number $\overline{Nu}$ of the downstream/upstream tube are correlated in the following form

$$\overline{Nu} = c_s\, Re^{m_s}\, Pr^{0.4} \tag{2}$$

and the tube side overall heat transfer coefficients for the tube with/without insert are also correlated in the form of equation (2) where constants c_s, exponents m_s, and standard deviation σ_s are tabulated in Table 2. The subscripts s represent 1 and 2. '1' stands for down- or upstream tube and '2' stands for overall downstream and upstream tubes. The data for each case at the same Re_h and insert can be correlated with

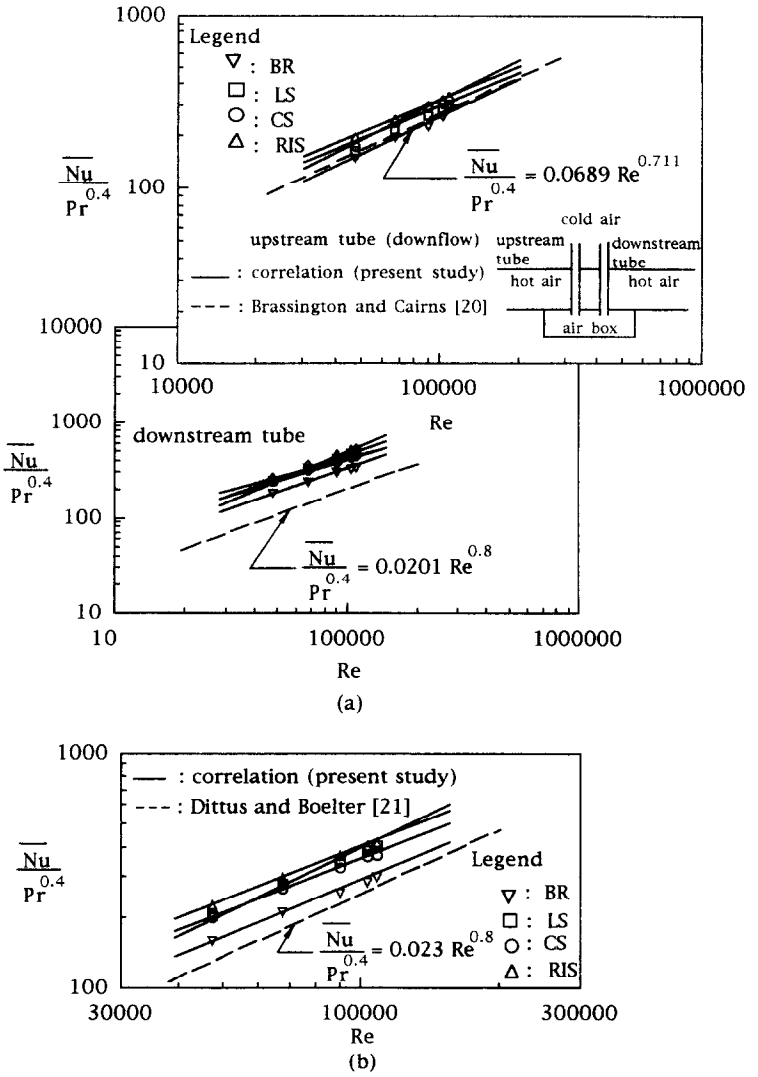

FIG. 6. Variation of (a) the individual dimensionless Nusselt number, (b) the average dimensionless Nusselt number, with Reynolds number for downstream/upstream tube.

a standard deviation of less than 0.47. The standard deviation is based on the difference between the calculation and experiment for the Nusselt number. These correlations represent the experimental data with a maximum error of 7.25%. At the 95% confidence level, $m = 0.74075 \pm 0.01828$. This shows that the Reynolds number dependence on heat transfer is not altered for all the four sets under consideration.

Table 2. Coefficients, exponents, and deviation, for heat transfer correlation of equation (2) and pressure drop factor of equation (5)

	Tube	c_1	m_1	σ_1	c_2	m_2	σ_2	c_3	m_3	σ_3
BR	downstream (upflow)	0.0382	0.779	0.136	0.0596	0.731	0.143	5.131	−0.143	0.091
	upstream (downflow)	0.0811	0.695	0.461						
LS	downstream (upflow)	0.0202	0.867	0.092	0.0503	0.781	0.447	6.895	−0.152	0.141
	upstream (downflow)	0.0829	0.715	0.469						
CS	downstream (upflow)	0.0491	0.795	0.124	0.0769	0.742	0.220	28.51	−0.276	0.396
	upstream (downflow)	0.144	0.667	0.108						
RIS	downstream (upflow)	0.0798	0.741	0.188	0.0983	0.709	0.370	17.25	−0.234	0.216
	upstream (downflow)	0.114	0.676	0.167						

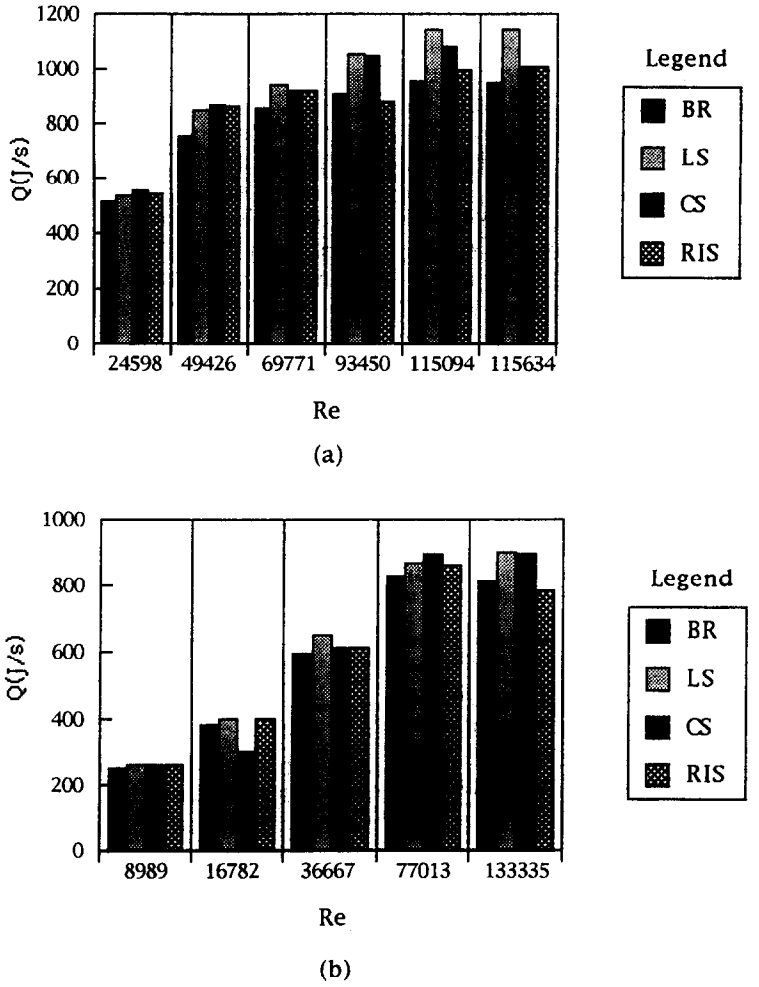

FIG. 7. Variation of the energy of heat exchange with Reynolds number based on (a) $T_{h,i} = 110°C$, (b) $T_{h,i} = 90°C$.

4.4. *The efficiency of heat exchange*

Figures 7(a) and (b) show the heat transfer based on the different inlet temperatures for hot air ($T_{h,i}$). It is shown that the tube with insert enhances the heat transfer with a gradual increase of the Reynolds number. Further examination of these two figures indicates that the heat transfer for the case of $T_{h,i} = 110°C$ increases about 15% compared to that of $T_{h,i} = 90°C$. Moreover, the mass flow rate for Re_c from 135 635 to 24 598 based on the tube without any insert is reduced about 81.9%, while the heat transfer is reduced only about 43.5%. This indicates that this type arrangement seems to have a better heat transfer under lower mass flow rates. This can also be evidenced in the following and shown in Table 1.

The ε–Ntu approach was applied to evaluate the efficiency of heat transfer for the present study. The results for these four different test tubes (BR, CS, LS and RIS) in counter-crossflow heat exchanger were also tabulated in Table 1. The ε from previous study [22] can be rewritten:

$$\varepsilon = \frac{1}{c}\left[1 - \frac{1}{1+(1-\phi_o/2)(e^{2c\phi_o}-1)}\right] \quad (3)$$

where $c = c_{min}/c_{max}$, and $\phi_o = 1 - e^{Ntu/2}$. The c_{min} and c_{max} are, respectively, the smaller and the larger of the two values of $c_{p,h}$ and $c_{p,c}$. Equation (3) was applied very well for a counter-crossflow with return bend heat exchanger. This type of heat exchanger is quite similar to that of present study. The major difference is that the 2-pass of the tube side is directly connected by U-bend, while present test tube of the 2-pass is inserted inside an air box (see Fig. 1). In order to further assess the reliability, a comparison between the present results and the results reported by ref. [22] was made. It can be seen that the error (E_1) shown in Table 1 compared with previous results [22] is less than 20%. This implies that the efficiency of heat transfer for the present study is higher than that in ref. [22]. Moreover, a close examination of the energy balance between the tube side and shell side shows that the error (E_2) is within the range of 10%. In

addition, it is also found that the effectiveness ε increases as the Ntu increases and capacity-rate ratio c_{min}/c_{max} decreases. This apparently indicates that the tube with insert increases the efficiency of heat transfer, and, in turn, increases the Ntu values. This coincides quite well with the above mentioned results (see Fig. 6(b)). When $c_{min}/c_{max} \leqslant 0.0405$ (i.e. about $Re_c \leqslant 25000$), it is found that the tube with RIS has the best efficiency of heat transfer, followed by CS, LS and BR, respectively. While $c_{min}/c_{max} > 0.0405$ (i.e. about $Re_c > 25000$), the tube with LS has the highest efficiency of heat transfer, the others are RIS, CS and BR, respectively. Naturally, the effectiveness ε of BR is usually smaller than those of the tubes with inserts.

4.5. *Pressure drop of the tube side*

The dimensionless pressure drop factor of the tube was calculated by the following equation

$$Eu = \frac{\Delta p}{\frac{1}{2}\rho v^2} \tag{4}$$

where Δp is the pressure drop of the tube side wind tunnel, v stands for the inlet velocity of cold air in the tube side channel. Figure 8(a) represents the variation of pressure drop factor in the tube side with the Reynolds number for the bare tube and for tubes with various inserts. A comparison of the present result for the bare tube and that of Bird *et al.* [23] has shown that the general tendency (the slope between log (Eu) and log (Re) remains nearly equal) can be considered satisfactory. However, the results for the bare tube of the present study are much higher than those of previous studies [23]. This difference seems due to the presence of the air box. In addition, the pressure drop factor for various fixed inserts is correlated in terms of the Reynolds number for the tube side in the form

$$Eu = c_3 Re_c^{m_3} \tag{5}$$

where constant c_3, exponent m_3, and standard deviation σ_3 are listed in Table 2. The data for each case at the same Re_h can be correlated with a standard deviation of less than 0.4. This correlation is based on the original data with a maximum of 8.16%. According to 95% confidence level, $m = -0.20125 \pm 0.01753$.

Furthermore, in order to estimate the increase of pressure drop due to the tube with inserts, the pressure drop ratio between the tube with fixed insert and the bare tube for different Reynolds numbers was made as shown in Fig. 8(b). This figure displays that, at $Re_c = 20000$, the pressure drop ratio for the CS-insert increases by 47% or so. While there are about 36 and 22% for both RIS- and LS-insert, respectively. At $Re_c = 130000$, an increase of the pressure drop could be reduced to 15 and 13%, respectively for the CS- and RIS-insert, while the LS-insert only slightly decreases to 21%. With a further increase of the Reynolds number, the increase of the pressure drop in the tube side was therefore reduced inversely, but nearly independent of Reynolds number for LS-insert. Making a comparison between CS- and LS-insert, when the Reynolds numbers $Re_c \leqslant 90000$, the CS-insert has a higher increase of pressure drop, but the tube with CS-insert would have a smaller pressure drop for the Reynolds numbers $Re_c > 90000$. In addition, with further comparison for the tube with RIS- and LS-insert, the tube with RIS has a larger pressure drop when the Reynolds numbers $Re_c \leqslant 70000$. On the contrary, when the Reynolds numbers $Re_c > 70000$, the tube with LS has a higher increase of pressure drop. Finally, comparing the RIS-insert with the CS-insert, it is found that the increase of pressure drop for the tube with CS-insert is higher than that of the tube with RIS-insert. According to the preceding results and discussions, it is found that the tube with RIS-insert may be an optimum selection for higher Reynolds numbers ($Re_c > 10^5$) as far as both the heat transfer and pressure drop are concerned.

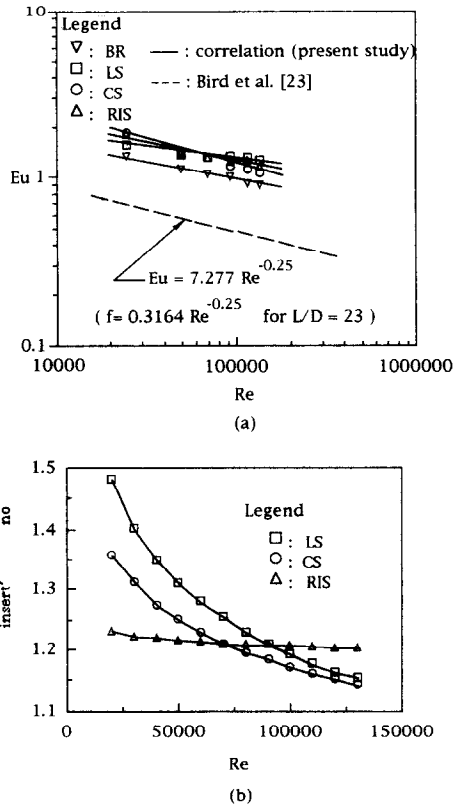

FIG. 8. Variation of (a) pressure drop factor; (b) pressure drop ratio with Reynolds number for the different test tube.

4.6. *Performance evaluation*

The performance evaluation for the present geometry with insert was based on the following two criteria developed by Bergles *et al.* [24].

Criterion 1. This criterion aims at increasing the heat transfer under the fixed basic geometry and fixed

pumping power of the heat exchanger. The performance ratio R_1 is given by

$$R_1 = \frac{(\overline{Nu})_{\text{insert}}}{(\overline{Nu})_{\text{fl}}} \tag{6}$$

where the subscripts 'insert' and 'fl' stand for the data of the test tubes with a partial insert and full-length insert, respectively. The equivalent smooth tube Reynolds number $(Re_c)_{\text{fl}}$ is estimated for equal pumping power in smooth tubes with inserts, and represented by the following

$$(Re_c)_{\text{fl}} = \left[\left(\frac{Eu_{\text{insert}}}{Eu_{\text{fl}}}\right)\left(\frac{A_{\text{insert}}}{A_{\text{fl}}}\right)\right]^{1/3} (Re_c)_{\text{insert}} \tag{7}$$

where

$$(A)_{\text{fl}} = (\pi/4)D^2$$

$$(A)_{\text{LS}} = (\pi/4)D^2 - \delta D$$

$$(A)_{\text{CS}} = (\pi/4)D^2 - 2\delta D + \delta^2$$

$$(A)_{\text{RIS}} = \frac{(A)_{\text{fl}} - 2\Delta\delta + (A)_{\text{LS}}}{2}.$$

Substituting $(Re_c)_{\text{fl}}$ and Eu_{fl} for $(Re_c)_{\text{BR}}$ and $(Eu)_{\text{BR}}$ into equation (5), the Eu_{fl} of the tube with insert for the equivalent bare tube can be calculated from the above substituted equation (5). Subsequently, by knowing the values of Eu_{insert}, $(Re_c)_{\text{insert}}$ and Eu_{fl}, the corresponding $(\overline{Nu})_{\text{fl}}$ of the tube with insert for the equivalent bare tube is then obtained by equation (2) for the bare tube. While the Nusselt number of the tube with insert $(\overline{Nu})_{\text{insert}}$ can be obtained by equation (2) for the tube of the fixed insert. According to the above calculations, the performance ratio R_1 can be therefore found.

Criterion 2. This criterion aims at reducing the pumping power for constant basic geometry and fixed heat duty. The performance ratio R_2 for this criterion is given by

$$R_2 = \frac{(Eu\, Re_c^3 A)_{\text{insert}}}{(Eu\, Re_c^3 A)_{\text{fl}}}. \tag{8}$$

The significance of the relative parameters in equation (8) is the same as that of equation (7). When $R_1 > 1$ it means that the heat transfer of the tube with insert is better than that of the bare tube, based on the equal pumping power. When $R_2 < 1$ under the equal heat transfer of the tube side, it expresses that the pumping power of the tube with insert is less than that of the smooth tube.

Figure 9 shows the thermal performance of three different inserts compared with bare tube, based on criterion 1 and criterion 2. The numerical data are also displayed on the figure. It is found that with a further increase of the Reynolds number Re_c the effect of enhancement for the tube with LS insert is increased. But the effect of enhancement is decreased for CS- and RIS-insert as the Reynolds number Re_c increases. Taking a closer examination of performance ratio R_1, the LS- and CS-insert could increase the heat transfer in the range of Reynolds numbers $Re_c = 25\,000$–$135\,000$. Moreover, at lower Reynolds numbers (Re_c), the tube with CS-insert has a better heat transfer enhancement. While at higher

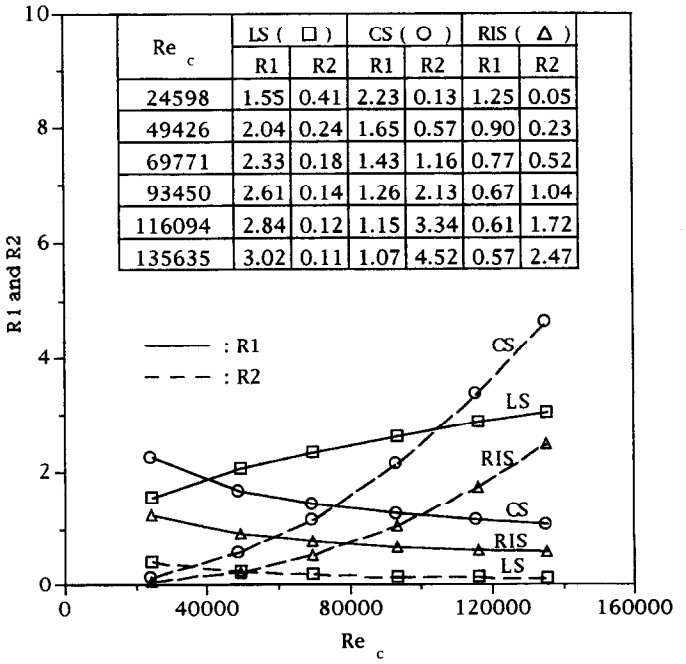

FIG. 9. Thermal performance of three type inserts compared with bare tube, based on criterion 1 and criterion 2.

Reynolds number (Re_c) the tube with LS has a higher enhancement than that of the tube with CS and the tube with RIS has the effect of augmenting the heat transfer only for $Re_c < 45000$. In addition, with an examination of the performance ratio R_2, the tube with LS could reduce the pumping power in the range of $Re_c = 25000$–135000. The tube with CS and the tube with RIS have the effect of reducing the pumping power only for the Reynolds numbers $Re_c < 65000$ and 90000, respectively, but the performance of the tube with RIS is much better than that of the tube with CS.

5. CONCLUSION

An experimental study of heat transfer enhancement and pressure drop in a vertical 2-pass tube with different inserts through an air box in a counter-crossflow heat exchanger was made in the range of $Re_c = 9000$–135000, $Re_h = 4300$, $T_{h,i} = 110$ and 90°C. The strip type inserts used in the two test tubes include LS, CS and RIS. The flow and thermal field visualizations are conducted to give an insight into the physical phenomenon. The important results of the present study are remarked in the following:

(1) Flow visualization indicates that the air flow of the upstream tube results in two vortices in the air box. The strengths of these two vortices are increased with the increase of the Reynolds number Re_c. Consequently, the heat transfer between cold air in the tube side and hot air in the shell side at the top place of the air box is augmented dramatically.

(2) The fringes outside the test tube for the interferograms of the temperature field are closely packed for the test tube faced at the hot fluid flow, and are sparsely packed for the rear of the test tube. Simultaneously, the flow separation/recirculation occurred at the rear of the test tube. It strongly implies that the higher heat transfer occurred at the front of the test tube while the lower heat transfer is present at the rear of the test tube. In addition, the interferograms for the fluid inside the BR show that the isotherms follow an approximate 'M-type' distribution. Its minimum temperature locates at the center between the center of the test tube and its bottom. The inner wall (especially near the lower wall) presents a higher temperature gradient. The thermal stratification was found at the upper core region. Furthermore, the temperature field around the outside of the test tube was not clearly influenced by the different inserts at the same Re_h and Re_c.

(3) Four sets of correlations for the average Nusselt number $\overline{Nu}$ (equation (2)) and four sets of correlations for pressure drop factors Eu (equation (5)) in the tube with/without various strip inserts are developed.

(4) When $c_{min}/c_{max} \leqslant 0.0405$ (i.e. about $Re_c \leqslant 25000$), it is found that the tube with RIS has the best heat transfer efficiency, followed by CS, LS and BR, respectively. While $c_{min}/c_{max} > 0.0405$ (i.e. about $Re_c > 25000$), the tube with LS has the leading heat transfer efficiency, followed by RIS, CS and BR, respectively. However, it can be seen that the effectiveness ε of BR is usually smaller than that of the tube with insert.

(5) Examination of performance ratio R_1, the LS- and CS-insert would increase the heat transfer in the range of Reynolds numbers $Re_c = 25000$–135000. Moreover, at lower Reynolds number (Re_c) the tube with CS-insert has a better heat transfer enhancement. While at higher Reynolds number (Re_c) the tube with LS has a higher enhancement than that of the tube with CS and the tube with RIS has the effect of augmenting the heat transfer only for $Re_c < 45000$. In addition, examination of performance ratio R_2, the tube with LS would reduce the pumping power in the range of $Re_c = 25000$–135000. While the tube with CS and the tube with RIS have the effect of reducing the pumping power only for the Reynolds numbers $Re_c < 65000$ and 90000, respectively, but the performance of the tube with RIS is much better than that of the tube with CS.

Acknowledgements—The study was supported by the China Steel Corporation (R.O.C.) through Grant TRC-80-21 for which the authors express their sincere gratitude and thanks. Special thanks go to Mr W.-F. Chou for his early assistance in conducting the measurements.

REFERENCES

1. A. E. Bergles, Augmentation of forced-convection heat transfer. In *Turbulent Forced Convection in Channels and Bundles* (Edited by S. Kakac and D. B. Spalding), pp. 883–909. Hemisphere, New York (1979).
2. F. E. Megerlin, R. W. Murphy and A. E. Bergles, Augmentation of heat transfer in tubes by use of mesh and brush inserts, *J. Heat Transfer* **96,** 145–151 (1974).
3. S. B. Uttarwar and M. Raja Rao, Augmentation of laminar flow heat transfer in tubes by means of wire coil inserts, *J. Heat Transfer* **107,** 930–935 (1985).
4. L. S. Yao and S. A. Berger, Fow in heated curved pipe, *J. Fluid Mech.* **88,** 339–354 (1978).
5. J. Prusa and L. S. Yao, Numerical solution of fully-developed flow in heated curved tubes, *J. Fluid Mech.* **123,** 503–522 (1982).
6. J. Azzola and J. A. C. Humphrey, Developing turbulent flow in a 180° curved pipe and its downstream tangent, Report LBL-17681, Lawrence Berkeley Laboratory, Univ. California (1984).
7. M. Moshfeghiah and K. J. Bell, Local heat transfer measurements in and downstream from a U-bend, ASME paper no. 70-HT-82.
8. K. C. Cheng, T. Inaba and M. Akiyama, Flow visualization studies of secondary flow patterns and semicircular pipes, *Third Int. Symposium on Flow Visualization*, pp. 761–766, Ann Arbor, MI (1983).
9. K. C. Cheng and F. P. Yuen, Flow visualization studies on secondary flow patterns in straight tubes downstream of a 180 deg bend and in isothermally heated horizontal tubes, *J. Heat Transfer* **109,** 49–54 (1987).
10. K. C. Cheng and F. P. Yuen, Flow visualization studies on secondary flow patterns in isothermally heated horizontal tubes, *J. Heat Transfer* **109,** 55–61 (1987).
11. W. Aung and R. O'Regan, Precise measurement of heat transfer using holographic interferometry, *Review of Scientific Instruments* **42,** 1755–1758 (1971).

12. A. A. Zukauskas and R. V. Ulinskas, Efficiency parameters for heat transfer in tube banks, *Heat Transfer Engineering* **6**(1), 19–25 (1985).
13. K. S. Chang, C. J. Choi and C. H. Cho, Laminar natural convection heat transfer from sharp-edged horizontal bars with flow separation, *Int. J. Heat Mass Transfer* **31,** 1177–1187 (1988).
14. W. W. Yousef and J. D. Tarsasuk, An interferometric study of combined free and forced convection in a horizontal isothermal tube, *J. Heat Transfer* **103,** 249–256 (1981).
15. A. D. Carr, M. A. Connor and H. O. Buhr, Velocity, temperature, and turbulence measurements in air for pipe flow with combined free and forced convection, *J. Heat Transfer* **95,** 445–452 (1973).
16. A. M. Abdelmeguid and D. B. Spalding, Turbulent flow and heat transfer in pipes with buoyancy effects, *J. Fluid Mech.* **94**(2), 400–483 (1979).
17. J. D. Nackson and W. B. Hall, Influence of buoyancy on heat transfer to fluids flowing in vertical tubes under turbulent condition. In *Turbulent Forced Convection in Channels and Bundles* (Edited by S. Kakac and D. B. Spalding), pp. 613–640. Hemisphere, New York (1979).
18. J. W. Baughn, H. Lacovides, D. C. Jackson and B. E. Launder, Local heat transfer measurements in turbulent flow around a 180-deg pipe bend, *J. Heat Transfer* **109,** 43–48 (1987).
19. M. M. Ohad and E. M. Sparrow, Heat transfer in a straight tube situated downstream of a bend, *Int. J. Heat Mass Transfer* **32,** 201–212 (1989).
20. D. J. Brassington and D. N. Cairns, Measurements of forced convection heat transfer to supercritical helium, *Int. J. Heat Mass Transfer* **20,** 209–214 (1977).
21. F. W. Dittus and L. M. K. Boelter, Univ. Calif. (Berkeley) Pub., Vol. 2, pp. 443 (1930).
22. P. Paikert, Thermal rating. In *Heat Exchanger Design Handbook* 3 (Edited by B. M. Brienza *et al.*) pp. 3.8.5–3. Hemisphere, Washington D.C., (1983).
23. R. B. Bird, W. E. Stewart and E. N. Lightfoot, *Transport Phenomena*, Chap. 6. Wiley, New York, (1960).
24. A. E. Bergles, A. R. Blumenkrantz and J. Taborek, Performance evaluation criterion for enhanced heat transfer surfaces, *Proc. Int. Heat Mass Transfer Conference*, Vol. 2, pp. 239–243 (1974).